AIAA 96-3205

Operation of a Solid-Rod Cathode in a Low-Pressure Discharge

Keith D. Goodfellow
Jet Propulsion Laboratory
California Institute of Technology
Pasadena CA 91109

32nd AIAA/ASME/SAE/ASEE
Joint Propulsion Conference and Exhibit
July 1-3, 1996 / Lake Buena Vista, FL

Final Draft

High-Current Low-Pressure Cathode Operation*

Keith D. Goodfellow†
Jet Propulsion Laboratory
California Institute of Technology
Pasadena, California

Abstract

Cathode erosion is one of the life-limiting mechanisms in several classes of electric thrusters. Since cathode erosion depends strongly on the cathode temperature, a quantitative understanding of the effects of cathode operation on the cathode temperature is required. A pure tungsten cathode was sucessfully operated in an argon discharge at pressures of 1.5 and 3.0 kPa and current levels of 600, 1000 and 1400 A. The cathode temperature profiles were repeatable with the pure tungsten cathode in contrast to previous test using thoriated tungsten cathodes. Excellent agreement was observed between the two measurement techniques. Increases in the operating current and/or decreases in the pressure resulted primarily in increases in the arc attachment area with small increases in the cathode tip temperature. The variation of the attachment area with current and pressure was characterized by measuring the intensity distribution of an argon ion line near the cathode surface. An approximately linear relationship was observed between the current density and the cathode temperature. Also, an approximately linear relationship was observed between the effective work function and the cathode temperature. Excellent agreement was seen between the experimental data and the model predictions.

Introduction

The service life of thermionic cathodes is important for a number of high current discharge devices, particularly several classes of electric thrusters such as electrothermal arcjets and magnetoplasmadynamic (MPD) engines. Low thrust levels dictate burn times of several thousand hours, and the cathodes of these devices are often the life-limiting component. High-current cathodes are subject to failure modes which can be classified as either event consequent or the result of damage accumulation. Event consequent failures, such as cathode melting as a result of excessive resistive heating, are the result of a single catastrophic event and can be adequately characterized by testing alone. However, it is impractical to characterize the failure risk associated with damage accumulation failure modes by testing alone because of the extremely long test durations required to observe the failures. Validation of cathode service life under conditions where damage accumulation failure modes are critical therefore must rely heavily on modeling of the physics of failure. The role of testing is to identify the critical failure modes, validate the models of failure and provide information on the model input parameters such as material properties and operating environment.

High current cathodes are being studied at the Jet Propulsion Laboratory as part of the Advanced Propulsion Concepts program. The goal of the program is to develop long-lived cathodes and the analytical

*Member of the Technical Staff, Advanced Propulsion Technology Group

tools to validate their service life. Cathode erosion, which appears to be the dominant damage accumulation failure mode, has been shown to depend strongly on the cathode temperature [1], Therefore, part of this study is intended to provide a simple means of predicting the cathode temperature for various thruster operating conditions. In addition, the thermal characteristics of the electrodes must be known to compute the overall thruster thermal loads to the spacecraft. Models must also provide the appropriate boundary conditions at the cathode surface for models of the operating characteristics of the thruster. For example, the current contours within the magnetoplasmadynamic thruster cannot be specified independently of the cathode temperature distribution because the majority of the current is from thermionic emission. Since the cathode model boundary conditions also depend on the characteristics of the main plasma, the two models must be ultimately coupled to obtain an overall model of the cathode region of the thruster.

A series of models describing the cathode and plasma interaction are being developed. The cathode model consists of two parts, namely a near-cathode plasma model and a thermal model of the cathode[2,3,4,5]. The near-cathode plasma model connects the properties of the main plasma with the cathode. Specifically, given the plasma properties within a mean-free-path of the surface, the near-cathode model predicts the heat flux and current density to the cathode surface. With these boundary conditions and the traditional thermal transport mechanisms, the thermal model can IJrt'diet the temperature distribution within the cathode. Because of the interdependency of the two models, they must be solved simultaneously. The input parameters used by the model for the plasma consist of { the sheath voltage, the pressure, the ionization energy of the gas, the ion mass, the surface work function, and the surface temperature. The arc attachment area is also specified to limit the total current, which is calculated using the given attachment area and the calculated current density distribution. The thermal model inputs consist of the base temperature or heat flux, the convection coefficient and environmental temperature, the surface emittance and environmental temperature, and the material thermal conductivity and resistivity. A series of thermal models have been developed with different levels of approximation. The nonlinearities of the system equations can present numerical difficulties. The simpler, one-dimensional models can be used to provide starting points for the more complete two dimensional models, significantly reducing the computational time required. Although the quasi-two dimensional models provide a good first approximation, a two dimensional model is required for a detailed understanding of the processes involved.

The focus of the experimental part of the program is to test new cathode concepts, identify the critical failure mechanisms, provide a database of measurements to validate the cathode models, and determine the values of the critical model drivers such as work function and gas pressure. The purpose of this paper is to present a database of temperature profiles recently obtained over a range of ambient pressures and current levels for a cylindrical pure tungsten cathode. A significant variation in the cathode temperature distribution was observed in previous experiments using thoriated tungsten cathodes [6, 7,8]. In addition, the size of the attachment area and electron temperature were characterized to provide inputs to subsequent modeling efforts.

Experimental Apparatus

The cathode test facility is shown in the diagram in Fig. (1) The stainless steel vacuum chamber is 0.5 m in diameter and 2.4 m long and is composed of 4 water cooled cylindrical segments. In addition, a water-cooled copper liner has been inserted in the middle two segments to permit long-duration operation. As the schematic in Fig. (2) shows, the first segment forms the discharge chamber. A water-cooled, ring-shaped copper anode with a diameter of 7.6 cm is mounted on a flange located between and electrically isolated from the first two tank segments. The cathode fixture mounted on the vacuum chamber door is composed of two coaxial tubes electrically isolated from each other and the door with micarta rings. The inner tube serves as the cathode current feed and has a water-cooled cap on the end to which the cathode is clamped. The outer tube is electrically floating and has a water-cooled copper disk mounted on the end with an aperture through which the cathode protrudes. The propellant gas is injected between the two tubes and flows into

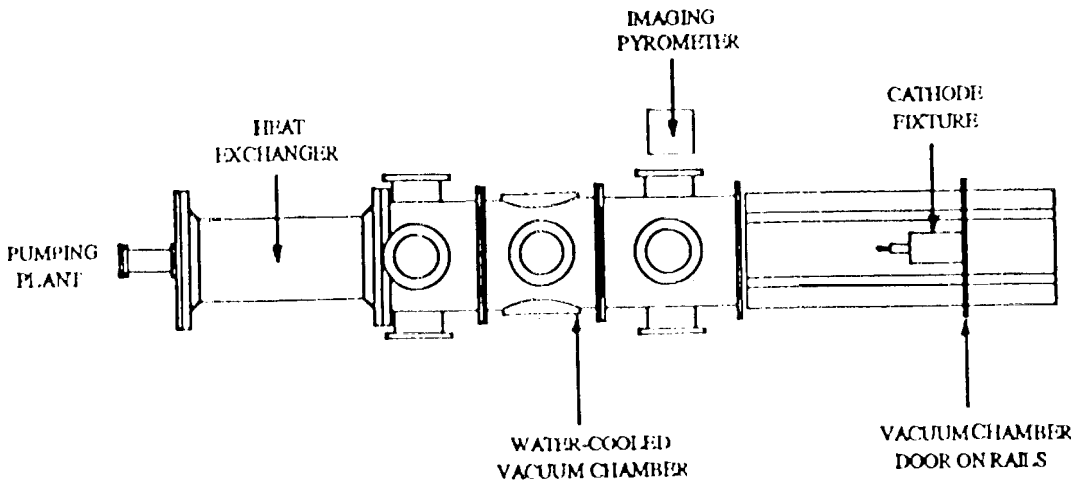

Figure 1: Diagram of the cathode test facility

the discharge chamber through an annulus around the base of the cathode. The interelectrode gap is set by the thickness of a spacer in the cathode assembly. The cathodes used in this investigation were rods of 2 percent thoriated tungsten 7 6 mm long and 9.5 mm in diameter with hemispherical tips. The last tank segment contains a heat exchanger made of water - cooled, finned copper tubing to cool the exhaust before it enters the pumping system. The tank has a number of ports which provide optical access to the discharge chamber as well as the plume. In addition, the cathode and the discharge can be viewed along the tank axis through a window at the rear of the tank.

The vacuum chamber is pumped by a 610 1/s Roots blower backed by a 140 l/s Stokes mechanical pump. The system is capable of achieving a vacuum of less than 0.13 Pa with no propellant flow and approximately 80 l'a with an argon flow rate of 0.75 g/s. Higher ambient gas pressures are achieved by throttling the pumping speed with a valve on a by pass around the main vacuum valve. The ambient pressure can be controlled to within approximately ±30 70 Pa The arc is powered by two Miller welding power supplies, each of which can provide 1500 **A** at a load voltage of 40 V continuously or 2000 A at 40 V with a 50 percent duty cycle. The initial arc breakdown is accomplished with a 4 A, 850 V start supply.

The factory shunts in the Miller welders have been replaced with precision shunts that are used to monitor the arc current. The terminal voltage is measured at the current feedthroughs into the tank. The propellant flow rate is measured with a Sierra Instruments Side-Trak Model 83[1 flow meter and a Micromotion Model D6 flow meter and controlled with a throttling valve located just upstream of the inlet to the cathode fixture. The flow meter output was calibrated by measuring the mass loss from an argon bottle as a function of time. Three M} '(S Barotron capacitance manometers with ranges of O 133 l's, O 1.3 x 10^4 l's, and O 1.3×10^5 l'a are used Lo monitor pressures. The three transducers are mounted in a single manifold with two input tubes. One line measures the tank pressure through a feedthrough on the chamber door. These parameters and a number of facility temperatures are recorded with a computer system

A CIDTEC ?250-1) Charge Injection Device (CID) camera was chosen as an optical pyrometric sensor to measure the two dimensional temperature field 011 the cathode. The system optics are composed of two interference filters with a 10 nm bandpass centered at 632.811111 and a long pass filter with a cutofl wavelength

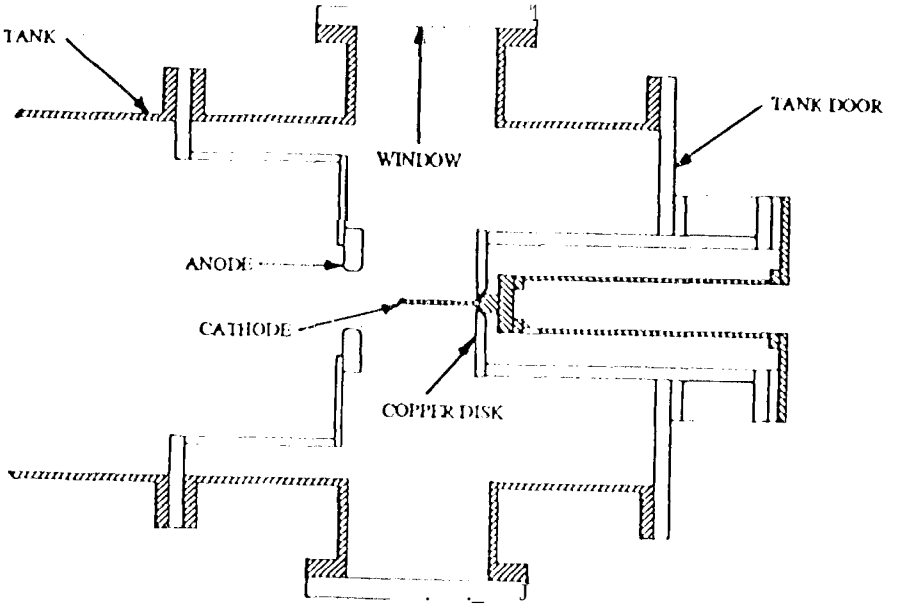

Figure 2: Schematic of the electrode configuration

of 570 nm The camera lens aperture is fixed at a relatively small value of f/4 and neutral density filters are used to control the image intensity. The imaging array has 512 x 512 CID detectors which are tead out at a maximum rate of thirty times per second, These values arc converted to an analog, signal, which is then further processed and output as a normal video signal by the camera electronics. The video signal is digitized by a Data Translation 1) '1 '-2862 8-bit frame-grabber board, which yields a final value between 0 and 255 corresponding to the incident power. The camera output was calib rated as a function of incident radiance using a tungsten ribbon lamp. The calibration procedure and a detailed error analysis for the temp erature measurements arc discussed in [6]. A surface emittance value of about O 57 was used for all thermal data analysis based 011 measurements made in Ref. [6].

In the experiments the camera and optics were mounted outside the chamber about 39.5 cm from the cathode. The video output from the camera was digitized to provide real time monitoring of the temperature distribution. One line in video memory chosen to correspond to the axis of the cathode was sampled from each frame. A given number of lines were averaged, displayed in real time, and periodically stored on disk.

The camera was also used to study the extent of the arc attachment region. Two interference filters with a 10 nm bandpass centered at 488 nm were used to select radiation from an intense argon ion line. Entire images of the cathode and near-cathode discharge region were then captured with the frame grabber board and analyzed to yield the lateral intensity distribution. These measurements were used to calculate an upper bound on the arc attachment area and the average current density in the attachment zone. The intensity scans were then Abel inverted to produce radial emittance profiles [9]. Filtering of the data was done within the Abel inversion routine using a FIR Blackman windowed filter.

Experimental Results

A series of experiments were performed using a pure tungsten cathode to eliminate the spatial and temporal variations in the surface work function that were observed with the thoriated tungsten cathodes [8, 5]. The tests were performed using argon gas at pressure levels of 1.5 and 3.() kPa, and for currents of 600, 1000 and 1400" A. The pressure was limited to 3.0 kPa and below because the model predicted that cathode

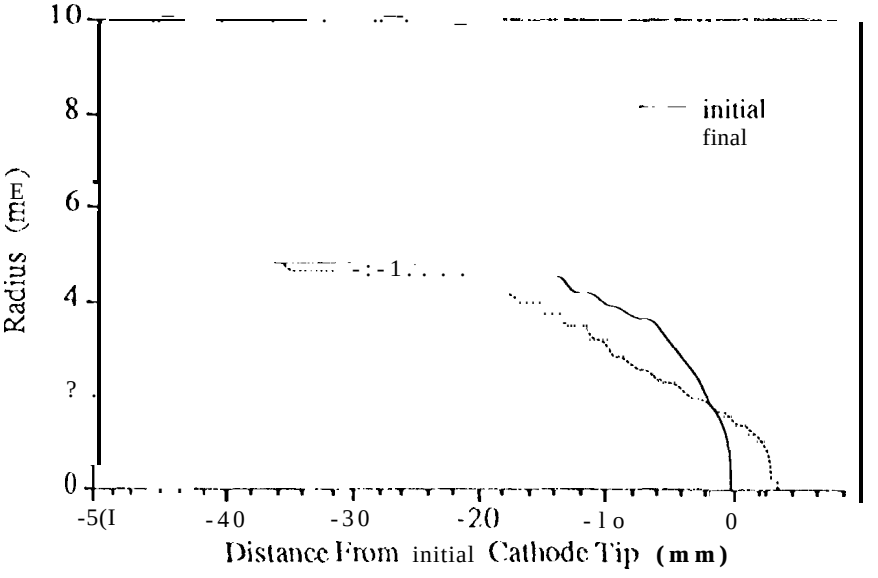

Figure 3 Pure tungsten cathode profiles.

melting would occur for the higher pressures and the high cathode tip temperatures measured during the tests confirmed this.

The cathode initially had a hemispherically shaped tip that became more "bullet shaped" as the tests proceeded. The initial and final profile shapes are shown in Fig. (3). Some of the material that evaporated from the sides was redeposited on the tip. The initial tip growth rate, determined from the camera images, was approximately 0.4 mm/hr but the rate had slowed to about 0.1 mm/hr at the end of the first series of tests. Cathode temperature and electron temperature scans were performed during each of the first series of tests, which lasted about three to six hours each. Negligible growth was observed during the second and third series of tests. The second and third series of tests lasted about one hour each, just long enough to obtain cathode temperature profiles. The pure tungsten cathode reached thermal equilibrium ($\geq$ 90 percent of final value) in two to three camera scans (30 seconds between scans) compared to about one hour for the thoriated tungsten cathodes. The long equilibration time for the thoriated tungsten cathodes is probably due to thorium migration on the surface [7,5].

The temperature profiles, shown in Figs. (4) and (5), for the second and third series of tests indicate that there is good repeatability in the cathode temperature measurements. The temperature profiles from the first series of tests were not used because of both the changing tip shape and a small shift in the transmittance of the window used for the imaging camera. The transmittance shift was probably due to tungsten evaporated from the cathode depositing on the window because cleaning the window restored the transmittance to its original value. No change in the window transmittance was observed during the camera calibrations that followed the second and third series of tests. All of the axial temperature profiles decrease monatonically as one moves from the cathode tip towards the base. This shape was also seen for the 4.5 and 6.0 kPa cases with thoriated tungsten cathodes, but for the 1.5 and 3.0 kPa cases a maximum in the temperature profiles existed a short distance from the tip [8, 5]. As shown in Fig. (4) arid Fig. (5) increasing the current causes an increase in the cathode temperatures away from the tip but does not significantly affect the tip temperature.

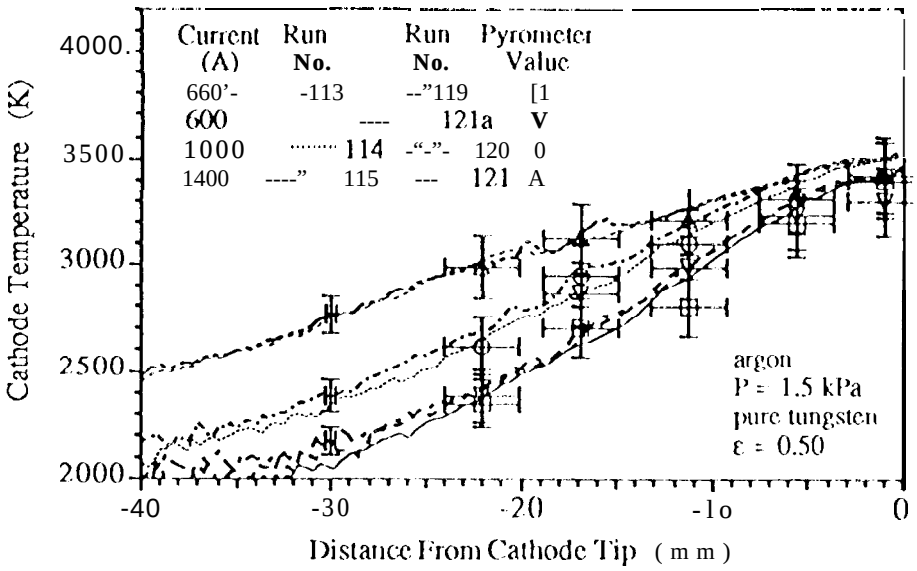

Figure 4: Pure tungsten cathode axial temperature profiles for a tank pressure of 1.5 kPa with current as a parameter.

That is, the attachment area increases more than the cathode temperature, or current density. Tests were limited to pressures of 3.0 kPa and less because for higher pressures the model predicted that the cathode tip would melt.

The markers shown with error bars in the cathode temperature plots are the measurements made with the Leeds and Northrup disappearing filament optical pyrometer. There is excellent agreement between the disappearing filament pyrometer measurements and the image camera measurements. This confirms that the camera is accurately determining the cathode temperature. At the cathode tip the disappearing filament pyrometer measurements are consistently low because these temperatures are near the upper end of its measurement range where it is less accurate. The spatial error bars are conservative estimates for the instrument pointing. The measurements could be accurately repeated for the locations near the cathode tip and the two furthest from the tip because marks on the cathode made them easy to locate. The spatial error bars are based on the second and third points which were more difficult to locate. The temperature error bars are based on a conservative estimate of 5 percent accuracy [10,11]. The error bars for the camera temperature profiles, that are located on the left side of the plot, were sized at ±3 percent [6,5]. A spatial error of plus or minus one pixel (0.298 mm) was used for all of the camera images. Both instruments and their respective vacuum tank windows were calibrated using the same black body calibration source.

The effect of changes in the tank pressure on the temperature profiles is shown in Fig. (6). Increasing the tank pressure raises the cathode tip temperature slightly and lowers the temperatures further from the tip), The same effect was observed in the thoriated tungsten cathode tests [5].

The extent of the arc attachment zone is an important parameter in the model because it determines what fraction of the boundary is subjected to the arc heat inputs and it is used computationally to limit the total current to the desired value. It is, of course, very difficult to measure directly the surface current density or the heat fluxes. In these experiments filter photography and emission spectroscopy were used to

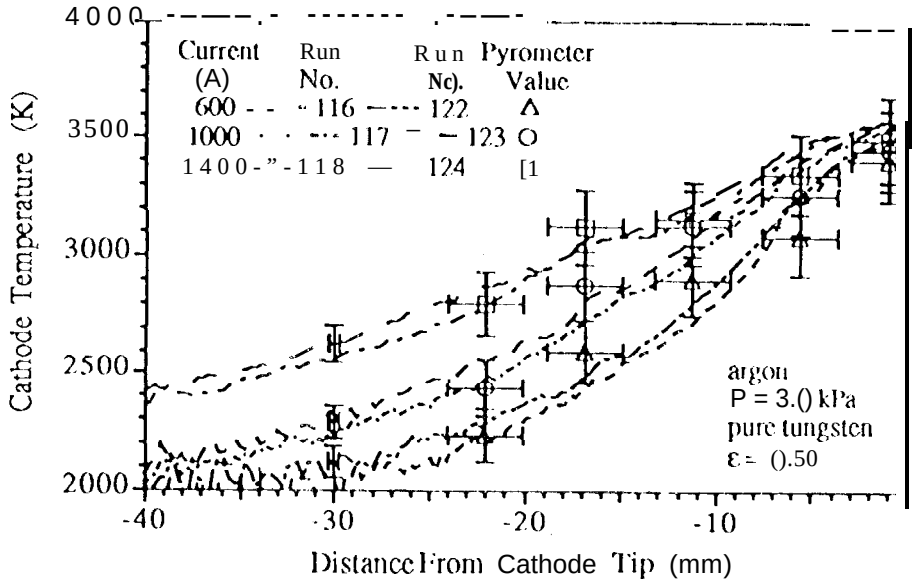

Figure 5: Pure tungsten cathode axial temperature profiles for a tank pressure of 3.() kPa with current as a parameter

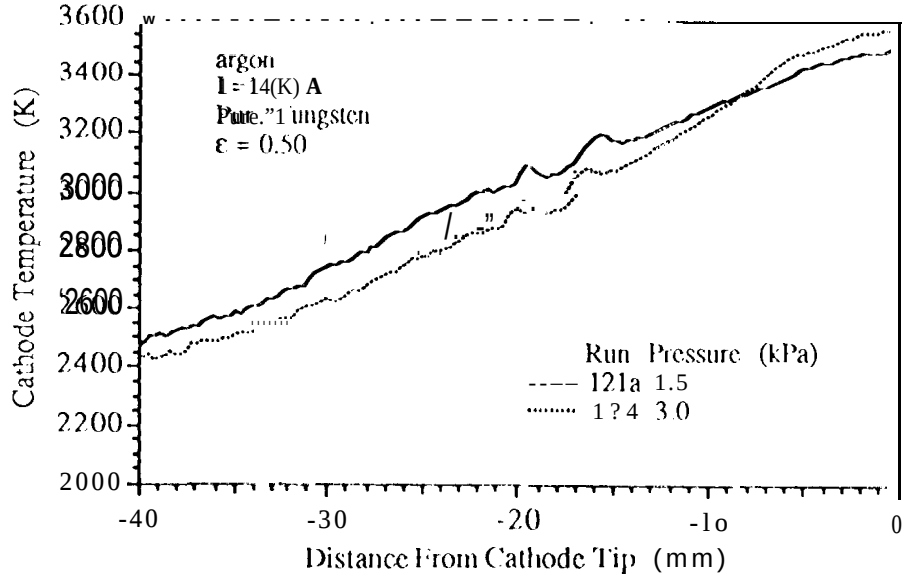

Figure 6: Pure tungsten cathode axial temperature profiles for a current of 1400 A with tank pressure as a parameter

Figure 7: Distribution of the 488 nm Ar II line intensity distribution at 6(KI A and 1.5 kPa for a pure tungsten cathode.

resolve the regions of most intense argon ion line emission and an estimate of the attachment area 011 the cathode surface.

Example contour plots of the 488 nm brightness levels are shown in Figs. (7) and (8). The contour levels represent the same brightness value for each plot. The first five contour levels are shown with higher values in increments of five units. The largest gradients for both cathode materials tested are on the side of the cathode near the tip. However, the gradients for the pure tungsten cathode are not as large or as concentrated as in the thoriated tungsten tests [8,5]. This indicates that the arc attachment is not as concentrated with pure tungsten as is expected from its larger work function. Also, increasing the current causes contours of any specific value to move closer to the base. That is, the arc attachment area increases with increasing current. The maximum contour values only change slightly, indicating that the maximum ion brightness does not change significantly with current. If one can assume that the brightness corresponds to ion density, then the local ion densities would not significantly change with current. Since the cathode tip temperature did not change significantly with current, the local current density is probably similar between current levels. Also, since similar conditions exist, the sheath voltages should be similar Therefore, since the ions are primarily produced from energy obtained by thermionic electrons passing through the sheath, equal to current density times the sheath voltage for a given length of time, one would expect a correlation between the cathode temperature and the ion brightness contours. Similarly, the expansion of the contours towards the cathode base with increasing current also agrees well with the cathode temperature results. That is, one would expect the ion brightness at a specific axial location to increase with an increase in the cathode temperature at that location. Similarly, the cathode temperatures arid the brightness contours expand closer to the cathode base for the 1.5 kPa tests than for the 3.(I kPa tests as one would expect. However, extreme care must be used in these assumptions because only one energy level transition is being considered, and the gas may not be in local thermodynamic equilibrium. Also, the ion number density is not a linear function of the current density.

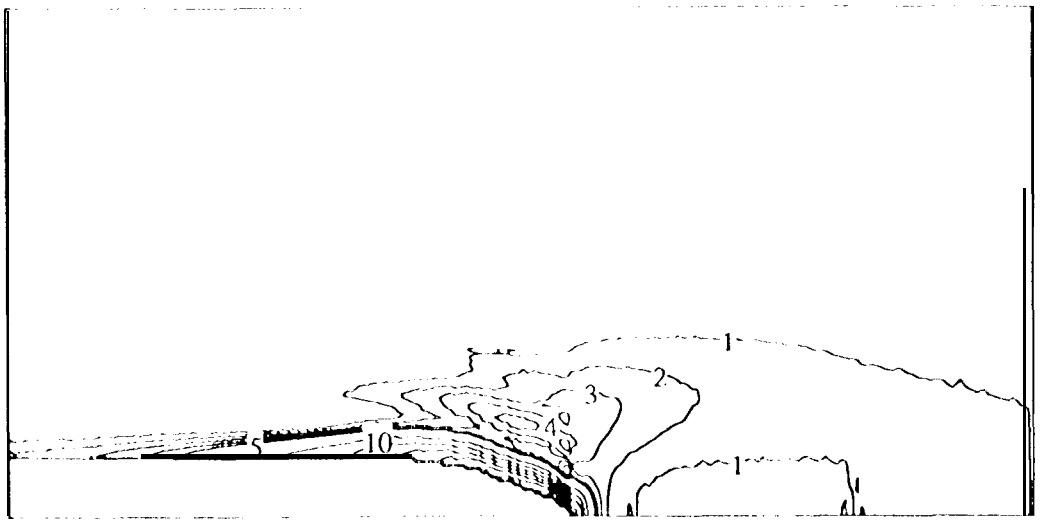

Figure 8. Distribution of the 488 nm Ar 11 line intensity distribution at 1400 **A** and 1.5 kPa for a pure tungsten cathode.

The cathode emission characteristics for each operating condition were calculated from the measured cathode temperature profiles. First, an average effective work function, presented in 'I'able (l), was calculated for each of the operating cases. The thermal image of each cathode was used to determine the radial edge

Pressure		Current	**(A)**
(kPa)	600	1000	1400
1.5	4.1694	4.1896	4.2045
3.0	4.1166	4.1334	4.1632

Table 1: Experimental effective work function values for pure tungsten cathode operation.

locations. These radial values were then used to compute the surface area for each axial location using a trapezoidal method. The area of the element at the tip includes both the side area and the tip surface area. Using the measured temperature profile, the surface areas and the total current, the average effective work function was calculated. This calculated work function includes both the material work function and any lowering conditions such as the Schott ky effect. The average effective work function increases with increasing current and decreasing pressure. Since the material work function is not expected to change for pure tungsten, these changes are probably due to changes in the electric field which in turn produces changes in the effective work function by the Schottky effect.

Using the calculated effective work function, the attachment areas corresponding to 25, 50, 75 and 98 percent of the total current were calculated. The attachment areas for the different enclosed currents and both pressures are shown in Fig. (9). All of the areas increase approximately exponentially with current.

For each attachment area and current combination, the cathode temperature, T_{Rich}, assuming that all of the current is from thermionic electron emission, was calculated using the Richardson equation. This temperature is the value the cathode would have if the attachment area had a uniform temperature. Therefore these temperature and area values can be used to compare the experimental results with the quasi-two dimensional cathode model.

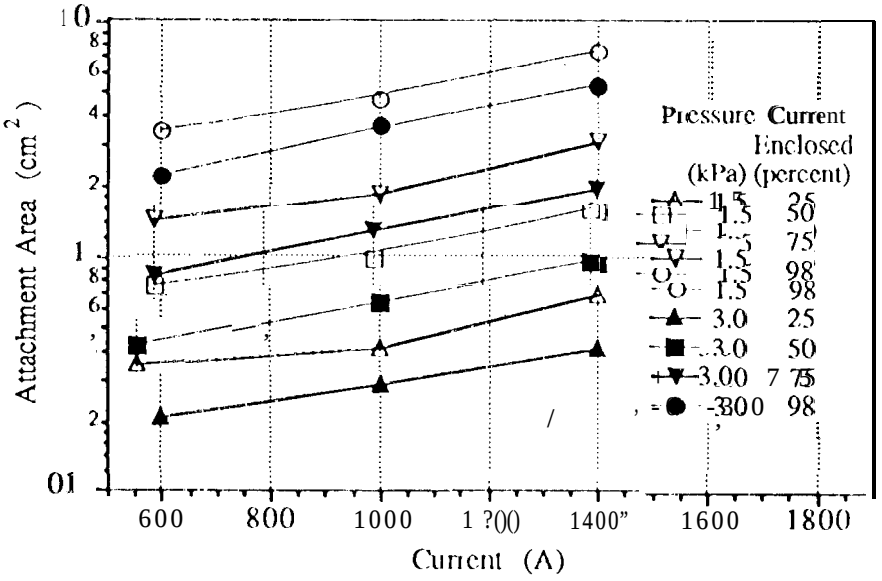

Figure 9: Arc attachment areas for pure tungsten cathode operation.

The correlation between the 48811111 Argon II line emissivity brightness and the calculated cathode current densities for all of the pure tungsten tests is shown in Fig. (10) The current densities were calculated using the measured cathode temperatures and the effective work functions talc.ulatccl above and given in Table (1). The 48811111 brightness values were those one pixel above the surface. The peaks on the right side of the plot are from the large brightness values observed near the tip. The curvature on the left side may be a camera effect. The brightness values for both the 488 nm images and the cathode temperature images for the left portion of the graph arc near the detection limit of the camera and therefore may contain significant errors. All of the values tend to fall on one characteristic curve, Since the major energy source for the ionization region is from thermionic electrons being accelerated through the sheath, one would expect there to be a correlation between these values. However, the exact correlation can not be determined I)r-cause both the sheath voltage and ion densities are unknown. A curve fit. to this data yields

$$\ln(\epsilon_{488}) = 0.6330 + 0.24878\ \mathrm{In}(j_b) - 0.03680\ [\mathrm{In}(j_b)]^2 \quad (1)$$

or

$$\ln(j_b) = -2.418 + 3.8412 \ln(\epsilon_{488}) - 0.4078\ [\ln(\epsilon_{488})]^2 \quad (2)$$

Model Predictions and Comparisons with Experiments

Near-Cathode Plasma Model

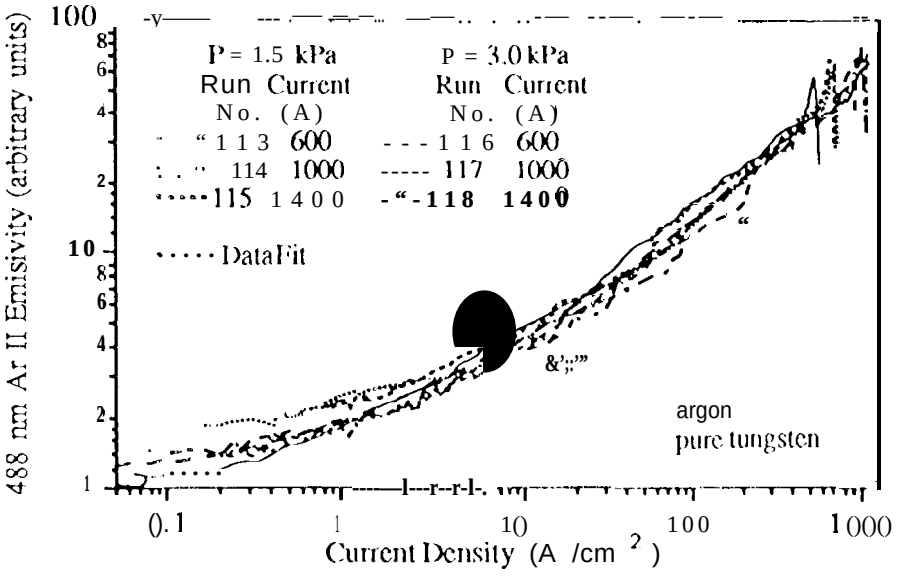

Figure 10: Brightness of the 488 nm Argon II line emissivity as a function of current density for the pure tungsten tests.

An illustration of the near-cathode plasma is shown in Fig. (1 1). The Debye length, mean free path, and thermal, concentration and momentum boundary layers are represented by L_D, L_{ei} and $L_{T,C,M}$ respectively. For this study, only the surface, sheath, presheath and ionization regions are modeled. In the main body of the plasma, the current is predominantly carried by the electrons, while in the sheath region the ion current may dominate. To match these regions an ionization region (which produces the required number of ions for the sheath region) is required between the sheath and the main plasma body. Similarly, a recombination region exists at the cathode surface to produce a transition to pure electron conduction in the solid. At the surface, ions are also converted to neutrals, which then return to the plasma. A complete description of each region model, the overall near-cathode plasma model and sample solutions are given in Refs. [8] and [5].

In general the cathode surface is characterized by the material, the surface finish and the temperature. For this model, the recombination region is assumed to be infinitesimally thin and is considered as a surface effect. Incident particles from the sheath heat the surface while emitted particles cool the surface. The energy balance at the surface balances the energy deposited and removed by the particles with heat conduction into the solid, and radiative, convective and mass (surface erosion) transport to the surroundings. The surface heat flux is the net of the energy deposited from the incident ions and plasma electrons, and the energy removed by the thermionic electrons. The incident ions tire recombined and reemitted as neutrals.

For high cathode temperatures, thermionic emission is the dominant current conduction mechanism in the near cathode region [12]. Thermionic emission is described by the Richardson-Dushman relation [13]. in addition, the surface electric field acts to enhance the emission, a phenomenon known as the Schottky effect [13]. The magnitude of the electric field at the cathode surface is primarily determined by the characteristics of the sheath region.

The sheath region is assumed to contain collisionless particles with constant total energy (potential plus kinetic). Six species are considered: monoenergetic thermionic or beam electrons, singly- and doubly-charged

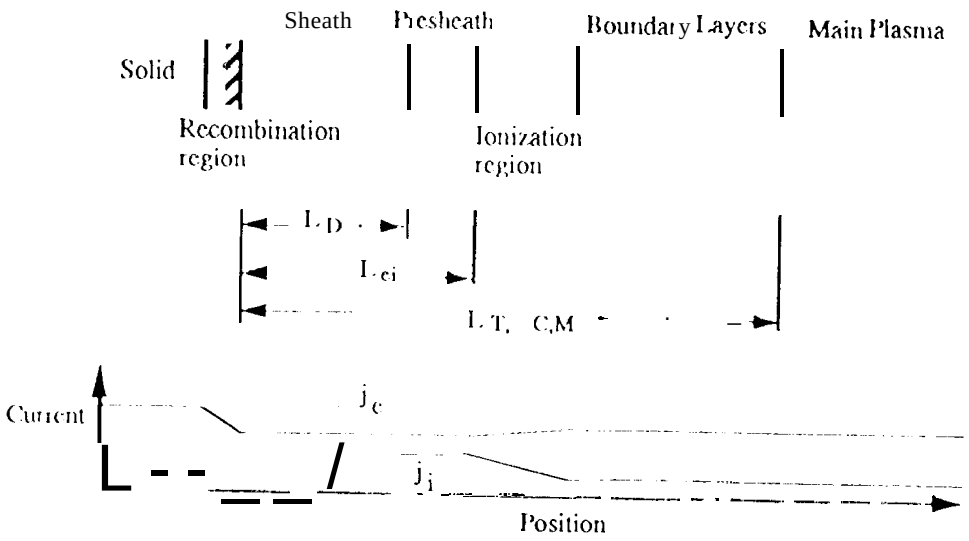

Figure 11: Near-catlloctc plasma regions.

monoenergetic ions for two monatomic gases, and Maxwellian electrons originating in the plasma [14,5]. Doubly-charged ions were added to a previously developed model [].5,2] because it has been suggested that cathode heating from doubly-charged ions may be significant at low pressures for high-current discharges [13]. Further, the sheath thickness is assumed to be much less than the Larmor radii of the particles, and therefore, magnetic field effects on the particle trajectories arc negligible.

For a stable sheath to occur, the ions must enter the sheath with energies equal to or greater than the Bohm minimum energy [16]. The ions here are assumed to enter the sheath with energies equal to the Bohm minimum energy which is represented as the Bohm potent ial. The plasma electrons are assumed to be Maxwellian arid referenced to the electron density at the sheath edge. These electrons fall into two classes, namely those with sufficient kinetic energy to overcome the sheath retarding potential and reach the cathode surface and those with insufficient energy that arc repelled back to the main plasma The corresponding flux of the high energy electrons constitutes the plasma electron current. The one-dimensional Poisson charge equation is used to describe the electric field and the electric potential

The ionization and presheath regions connect the sheath region with the main plasma body [17] [13]. The purpose of the presheath region is to accelerate the ions so that they enter the sheath region with the minimum energy required for a stable sheath (Bohm energy) [16]. For this model the presheath region is combined with the ionization zone by requiring that ions leave the ionization region with the Bohm energy. The ionization region generates the required number of ion and electron pairs to match the sheath and main plasma body values. The plasma temperature is determined from the energy balance and the particle number densities are determined by the Saha equation (equilibrium ionization/recombination) [5].

The data from the low-pressure experiments with the pure tungsten cathode compare well with the model predictions. The model predictions for a cathode with the same geometry as the experimental ones and a work function of 4.35 eV [18] are shown in Figs. (12) through (15). The work function reduction predicted by the model for these operating conditions is about 0.15 eV. Two types of comparisons were made. The results for both comparisons arc presented in Table (2) First, the attachment area for the experimental data was matched to the model attachment area value corresponding to the local minimum in the effective work function. The value of T_{Rich} was then determined using the experimental area and the experimental

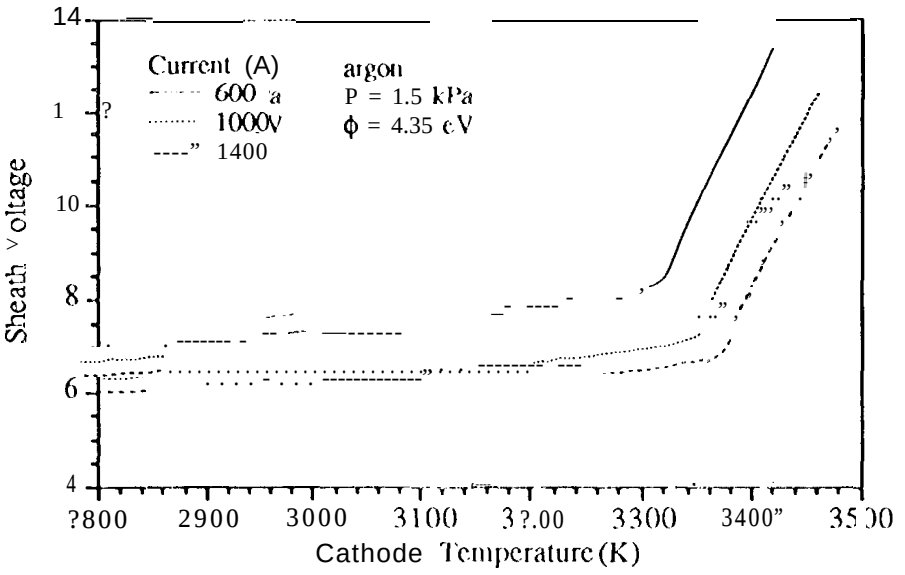

Figure 12: Sheath Voltage as a function of cathode temperature for a pure tungsten cathode and a pressure of 1.5 kPa with current as a parameter.

effective work function. Recall that the experimental effective work function is determined from the cathode temperature distribution and the total current. The relative differences for the two temperatures are 0.21, 0.15 and 0.27 percent for 600, 1000 and 1400 A, respectively. The differences in the effective work functions were 0.49, (),10 and 0.20 percent, respectively. The model electron temperatures and sheath voltages are also consistent with measured electron temperatures and arc voltages. The excellent agreement between the two effective work functions indicates that the model is properly determining the surface electric field for the Schottky effect. The agreement between the temperatures indicates that the Richardson equation is properly determining the thermionic emission current density and that the majority of the total current is carried by the thermionic electrons. However, this method dots not produce a repeatable amount of enclosed current. The enclosed current values fell between 70 and 85 percent for all of the pure tungsten experiments, but there is no apparent correlation between enclosed current percentage and either total current or pressure. This method is capable of predicting cathode operational characteristics since no additional information is needed.

For the second comparison, the experimental attachment area corresponding to 98 percent of the enclosed current was determined. Then the cathode temperature in the model was adjusted to give a comparable attachment area. The relative differences for the two temperatures are 0.68, 0.89 and 0.94 percent for 600, 1000" and 1400 A, respectively. The differences in the effective work functions were 1 14, 0.63 and 0 46 percent, respectively. Although the differences are slightly larger for this comparison they are still typically less than one percent. **It was** expected that the differences with this method would be lower than for the first method since the cathode conditions for 98 percent of the enclosed current should be close to those for the entire cathode (100 percent of the current). The problem with this technique, however, is that the attachment area corresponding to 98 percent of enclosed current is not known a-priori. For predicting operational characteristics, an additional model, such as an arc column model, would be needed to determine

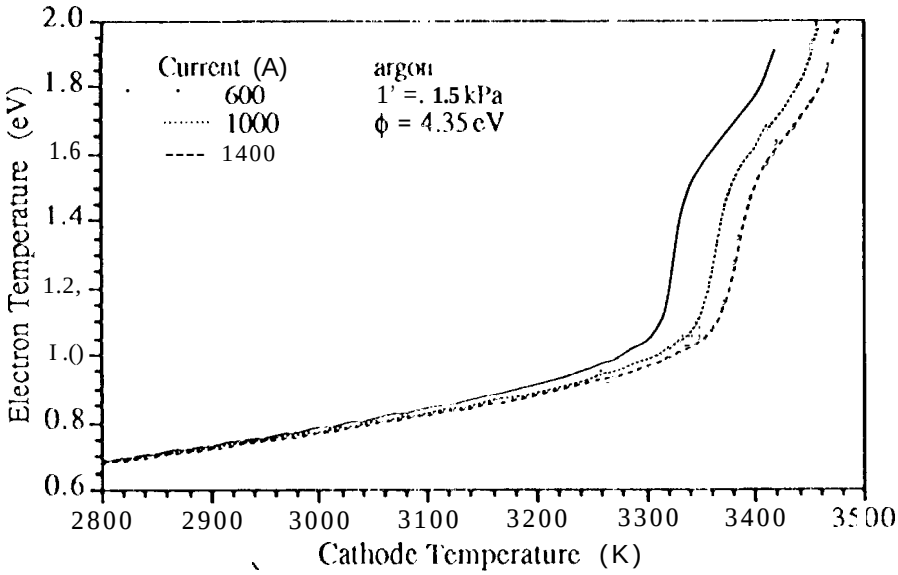

Figure 13: Electron temperature as a function of cathode temperature for a pure tungsten cathode and a pressure of 15 kPa with current as a parameter.

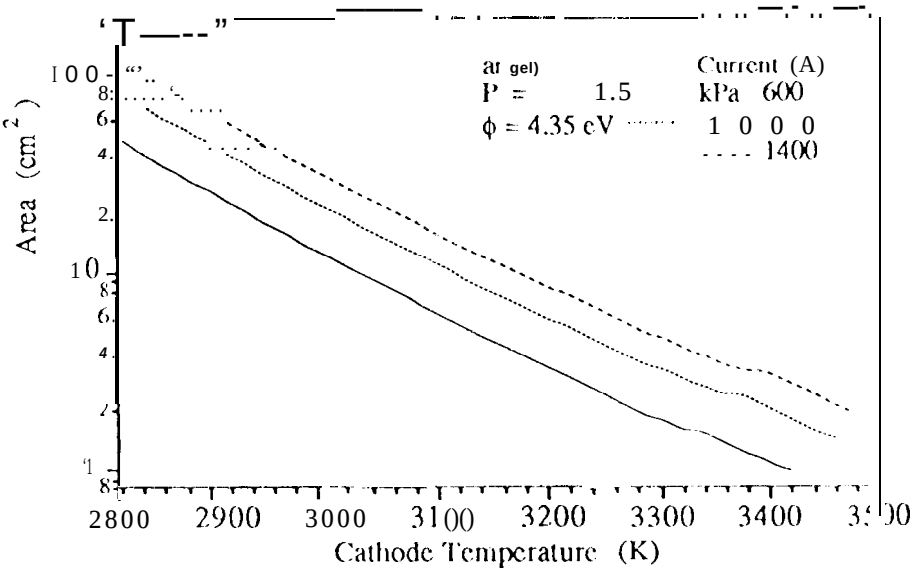

Figure 14: Attachment area as a function of cathode temperature for a pure tungsten cathode and a pressure of 15 kPa with current as a parameter.

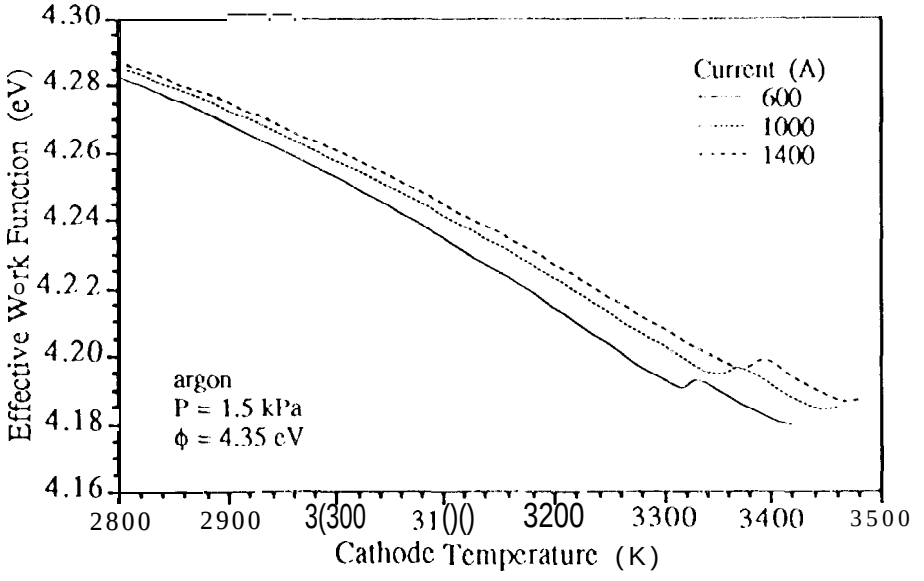

Figure 15 Effective work function as a function of cathode temperature for a pure tungsten cathode and a pressure of 1.5 kPa with current as a parameter.

I_{tot} (A)	ϕ_{min} T_c (K)	Model V_c	Soln. T_e (eV)	A_{attach} (cm^2)	ϕ_{eff} (eV)	A_{attach} (cm^2)	Expt. ϕ_{eff} (eV)	Data T_{Rich} (K)	I_{encl} (%)
600	3321	8.450	1 1490	1..5479	4.190	1.5426	4.169	3328	80
1000	3355	7.605	1 1393	2.331	4.194	2.427	4.190	3360	85
1400	3374	7.201	1.1360	3.086	4 196	3.041	4 204	3365	75
	Area	Match	Model	Soln.		Expt.	Data		
600	3186	7.757	0 8942	3.391	4.217	3.386	4 169	3208	98
1000	3233	7.047	0 9103	4.556	4.216	4.564	4.190	3262	98
1400	3218	6.619	0 8876	7.234	4 229	7.237	4.204	3248	98

Table 2: Model solutions and experimental data for the pure tungsten cathode configuration at 1.5 kPa

the attachment area.

The same two methods were used for comparisons with the tests at a pressure of 3.0 kPa. The comparisons are presented in Table (3). For the minimum work function comparisons, the relative differences between the model cathode temperature and T_{Rich} are 0.84, 1.28 and 1.09 percent for 600, 1000 and 1400 A, respectively. The differences in the effective work functions were 1.04, 0,76 and 0.112 percent, respectively. For the 98 percent enclosed current comparison the relative differences between the model cathode temperature and T_{Rich} are 0.043, 0.061 and 0.34 percent for 600, 1OO() and 1400 A, respectively. The differences in the effective work functions were 2.0, 1.76 and 1.18 percent, respectively. Again, the model electron temperatures and sheath voltages are also reasonable for both comparisons.

	$\phi_{\min}$	Model	Soln.				Expt.	Data	
I_{tot}	T_e	V_c	T_e	A_{attach}	ϕ_{eff}	A_{attach}	ϕ_{eff}	T_{Rich}	I_{encl}
(A)	*(1f)*		*(c'\')*	(cm^2)	(eV)	(cm^2)	(c\')	(K)	(%))
600	3434	8.696	1.1847	0.8050	4.160	0.812-('	4.117	3405	75
1000	3474	7.793	1.1844	1.2035	4.165	1.2512	4.133	3430	75
1400	3497	7.369	1.1864	1.5845	4.168	1.5987	4.163	3459	70
	Area	Match	'Model	Soln.		Expt.	Data		
600	3256	7.859	0.8975	2.192	4.201	2.192	4.117	3255	98
1000	3272	7.033	0.8888	3.582	4.208	3.582	4.133	3270	98
1400	3271	6.627	0.8783	5.243	4.213	5.247	4.163	3282	98

Table 3: Model solutions and experimental data for the pure tungsten cathode configuration at 3.0 kPa

The results from the two dimensional model were not significantly different from those of the quasi-two dimensional model for the operating conditions considered here. The cathode centerline and surface temperature for two example cases are shown in Fig. (16). As expected the radial temperature variations are small compared to the axial ones. For all of the model solutions the cathode temperatures were uniform in the arc attachment area. The temperature variation was usually less than 50 K. Near the tip, the surface temperature is higher than the centerline value because of the surface heating from the arc attachment. At the tip the two temperatures are closer because of the arc attachment. Upstream of the attachment area the centerline temperature is higher than the surface temperature because of the radial cooling due to radiation.

A comparison between the experimental data and two model solutions are shown in Fig. (17). Again, the value of the base temperature was selected to give a reasonable match to the experimental data near the cathode base. The model was not sensitive to these adjustments, arid values of 1500 and ?000 K produced similar results, The cathode tip temperatures agree quite well even though the model currents were larger. As with the previous temperature profile comparisons, the model predicts a faster decrease in the cathode temperature as one moves towards the cathode base. Although the model agrees well with the experimental data, it is still not capable of accurately predicting behavior at other conditions because the attachment area and the sheath voltage are not known.

The data from both the pure and thoriated tungsten cathode tests were used to estimate the correlations between the cathode temperature, the effective work fullc.tier] and the current density. The current density is shown as a function of the cathode temperature in Fig. (18). The continuous lines show the current density predicted from the Richardson equation for different effective work functions. The symbols indicate the data from all of the tests presented in this section. The cathodes for this range of operating conditions appear to operate such that the current density slowly increases with cathode temperature. This trend is significantly

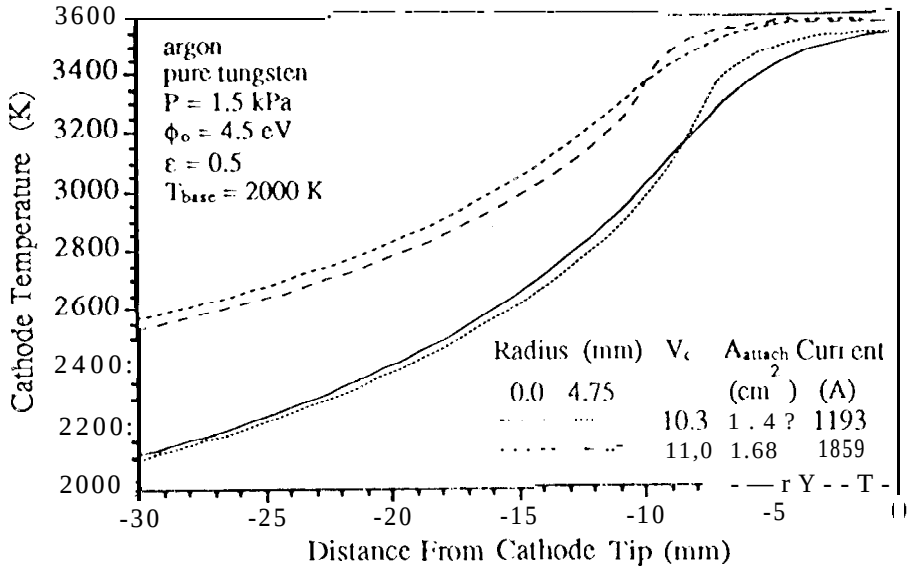

Figure 16 : Cathode surface and centerline temperatures as a function of axial position for a pure tungsten cathode and a pressure of 1.5 kPa.

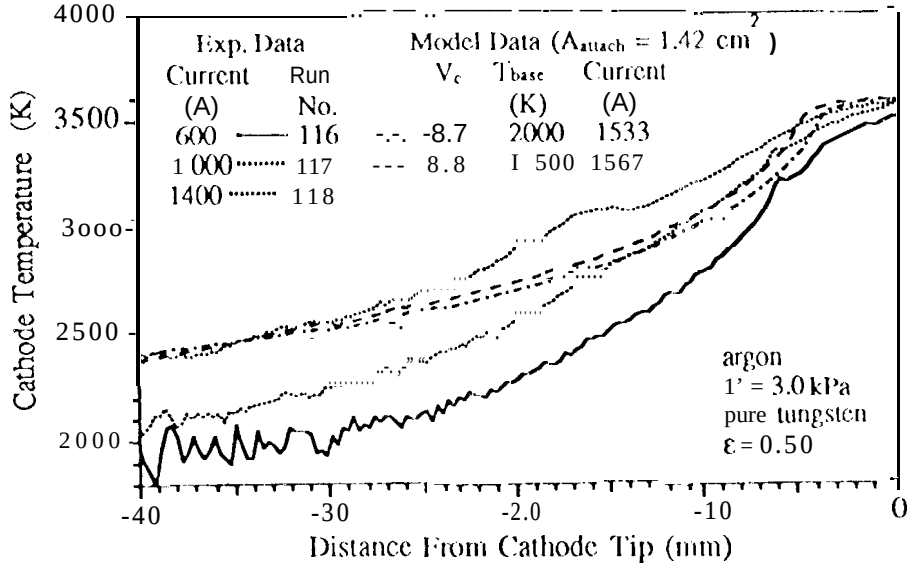

Figure 17: Cathode surface temperature as a function of axial position for a pure tungsten cathode and a pressure of 3,0 kPa.

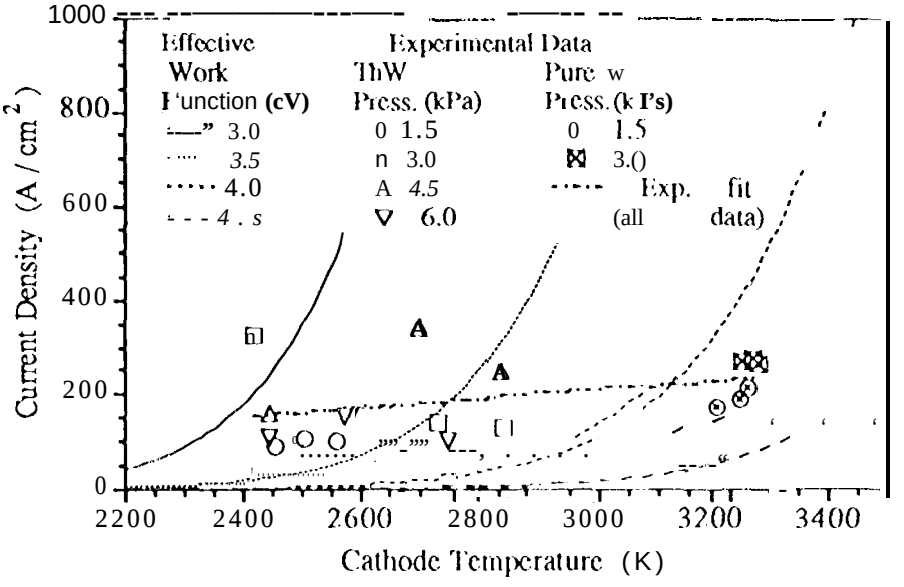

Figure 18: Current density as a function of cathode temperature

different from what is predicted using the Richardson equation. The pure tungsten data have a shape similar to the Richardson equation lines over a small range, but the thoriated tungsten data do not.

The effective work function is shown as a function of the cathode temperature in Fig. (19). The experimental data and the model predictions using the 98 percent enclosed current area are shown with the symbols, and agree well. A linear fit to all of the experimental data is also shown. It appears that when all of the operating parameters, sue]] as attachment area, sheath voltage, electron temperature and surface electric field are considered, that there is a linear relationship between the effective work function and the cathode temperature.

The curved lines in Fig. (19) arc predictions from the model using the minimum effective work function point discussed previously. Although these model predictions have the same shape arid similar slopes, they predict higher cathode temperatures for a given effective work function value than was observed in the experiments. This further confirms that the minimum effective work function point may represent an upper bound on the operation, but dots riot represent the average values. That is, for some of the operating points, the conditions near the tip where the cathode temperature is the largest, may be represented by the minimum effective work function point. Therefore, this method may be useful for predicting operation at the hottest or highest erosion location of the cathode.

The primary erosion mechanisms for steady-s(ate cathode operation arc dependent on the cathode operating environment. For low discharge pressures where the gas transport processes can be neglected, the evaporation rate can approach the vacuum evaporation rate. As the pressure is increased, the gas transport process become increasingly important and the erosion process is diffusion-limited. The presence of oxygen, even in small quantities, can significantly increase the erosion rate through the formation of volatile tungsten oxides. Tests performed by Polk [19] measured erosion rates that were approximately an order of magnitude less that the rates predicted by the vacuum evaporation rate indicating that diffusion processes were present. These tests also revealed an order of magnitude increase in erosion when poorer gas purity was used.

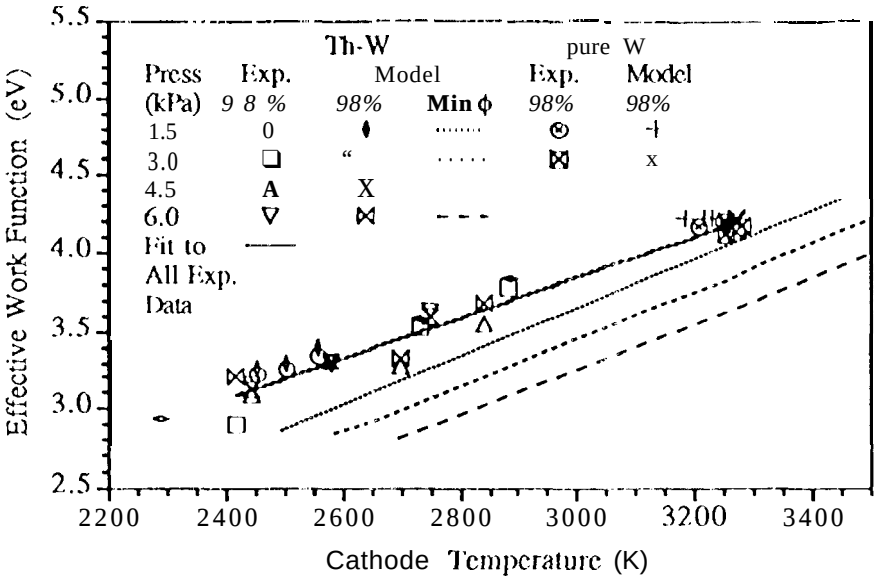

Figure 19: Effective work function as a function of cathode temperature

The vacuum evaporation rate was used as an upper bound prediction for these experiments [19]. The vacuum evaporation rate for tungsten is strongly dependent 011 the cathode temperature. For the thoriated tungsten cathode tests the cathode temperatures were typically 2600 2800 K which correspond to erosion rates of 0.0090 0.113 $\mu g/cm^2 s$ while the pure tungsten cathode tip temperatures were typically 3400 3600 K which correspond to erosion rates of 81- 167 $\mu g/cm^2 s$. Therefore, a factor of 1.3 increase in cathode temperature produces roughly a factor of 1500 increase in erosion rate. The vacuum evaporation rates for the pure tungsten cathodes are shown in Fig. (20). For each temperature profile, the local evaporation rates were calculated and then combined with the local surface areas to predict the total cathode erosion. The total evaporation rates increase with current but do not appear to be pressure dependent as seen in Fig. (20). Recall that increasing the current anti/or decreasing the pressure resulted in an increase in the arc attachment area and an increase in the overall cathode temperature. For the pressure increases, however, the tip temperature decreased slightly. The increase in the temperature and erosion rates towards the cathode Last appear to be offset by the cathode temperature and erosion rate decreases at the cathode tip. Although the cathode tip area is smaller, the temperatures were the greatest and therefore temperature changes here would have a larger effect on the erosion rate. The total mass lost during the pure tungsten cathode tests was 2.098 g in 19.12 hours with an average current of 961 .3 **A** for an average mass loss rate of 110 mg/hr. The vacuum evaporation rate prediction for this operation was 4 841g which is a factor of 2.31 higher than the actual mass loss.

Acknowledgements

The research described in this paper was conducted at the Jet Propulsion Laboratory, California Institute of Technology, under a contract with the National Aeronautics and Space Administration.

The author would like to thank Jay Polk and John Brophy for the technical advice arid Bill Thogmartin, Bob Toomath and Al Owens for their technical assistance with the cathode test facility.

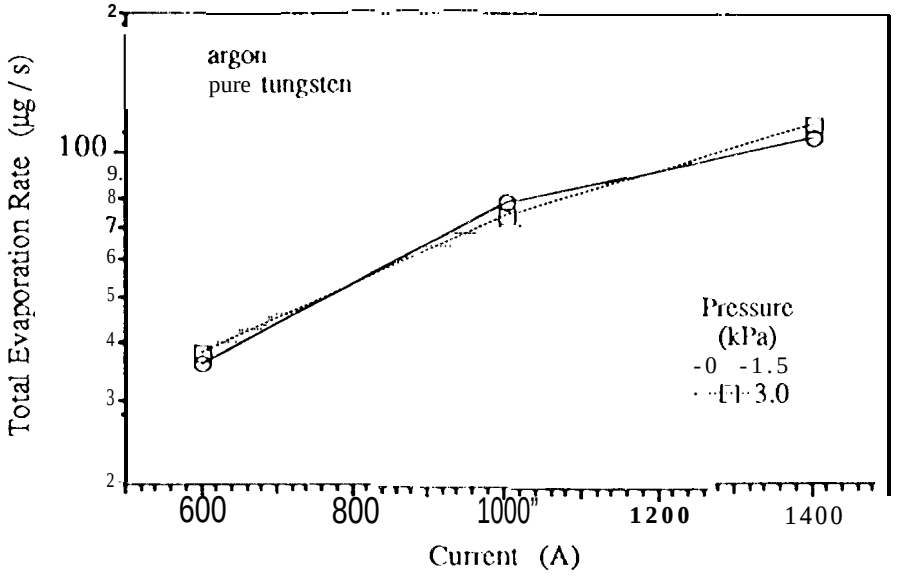

Figure 20: Cathode evaporation rates for pure tungsten cathode tests

References

[1] J. E. Polk, **A. J.** Kelly, **and** R. G. Jahn. Mechanisms of Hot Cathode Erosion in MPD Thrusters. In 21st *International Electric Propulsion Conference*, Orlando, FL, 1990. AIAA-90-2673

[2] K. D. Goodfellow and J. E. Polk. High Current Cathode Thermal Behavior, Part I: Theory. In 23rd *International Electric Propulsion Conference*, Seattle, WA, 1993. IEPC 93-030.

[3] K. D. Goodfellow and J. E. Polk. Theoretical Operation of Solid Rod Cathodes. In 30th *Joint Propulsion Conference*, Indianapolis, IN, 1994. AIAA 94-3132.

[4] K. D. Goodfellow. Theoretical Investigation of Cathode Operation in High-Power Ammonia Arcjets. In 31st *Joint Propulsion Conference*, San Diego, CA, 1995. AIAA **953061.**

[5] K. D. Goodfellow. *A Theoretical and Experimental Investigation of Cathode Processes in Electric Thrusters.* PhD thesis, University of Southern California, Los Angeles, CA, USA, 1996.

[6] J. E. Polk and K. D. Goodfellow. High Current Cathode Thermal Behavior, Part II: Experiments. In 23rd *International Electric Propulsion Conference*, Seattle, WA, 1993. IEPC 93-029.

[7] J. E. Polk and K. D. Goodfellow. Experimental Investigation of Solid Rod Cathode Operation. In 30th *Joint Propulsion Conference*, Indianapolis, IN, 1994. AIAA 94-3131.

[8] K. D. Goodfellow and J. E. Polk. Experimental Verification of a High-Current Cathode Thermal Model. In 31st *Joint Propulsion Conference*, San Diego, CA, 1995. AIAA 953062.

[9] S. T. Sudharsana. The Abel Inversion of Noisy Data Using Discrete Integral Transforms. MS Thesis, The University of Tennessee, Knoxville, Knoxville, TN, USA, 1986.

10] D. P. DeWitt and G. D. Nutter. *Theory and Practice Radiation Thermometry*. John Wiley and Sons, New York, NY, 1988.

11] M. Cerezo. Jet Propulsion Laboratory / California Institute of Technology, Optical Standards Group, Pasadena, CA, 1996. Private Communication

D. Q. King. Feasibility of Steady-State Multi-Megawatt MPD Thrusters. In 18th *International Electric Propulsion Conference*, Alexandria, VA, 1985. **AIAA 85-2004,**

W. Neumann. *The Mechanism of the Thermoemitting Arc Cathode*. Akademie-Verlag Press, Berlin, Germany, 1987.

14] P. D. Prewett and J. E. Allen. The Double Sheath Associated with a not Cathode. *Proceedings of the Royal Society of London*, 348:435-446, 1976

15] K. D. Goodfellow, T. J. Pivirotto, and J. E. Polk. Applied-Field Magnetoplasmadynamic Engine Developments. in 28th *Joint Propulsion Conference*, Nashville, TN, 1992. AIAA 92-3293.

16] D. Bohm. *The Characteristics of Electrical Discharges in Magnetic Plasma*. McGraw-Hill, New York, NY. 1949.

W. L. Bade and J. M. Yes. Arcjet Technology Research and Development-Final Report. Technical Report NASA CR-54687, AVCO Corporation, Wilmington, MA, 1965.

V. S. Fomenko and G. V. Samsonov. *Handbook of Thermionic Properties*. Plenum Press, New York, NY, 1966.

J. E. Polk. *Mechanisms of Cathode Erosion in Plasma Thrusters*. PhD thesis, Princeton University, Princeton, NJ, USA, 1996.